Received: 10 November 2021 | Revised: 24 February 2022 | Accepted: 28 February 2022

DOI: 10.1002/pro.4295

FULL-LENGTH PAPER

THE PROTEIN SOCIETY WILEY

Multivalent Angiomotin-like 1 and Yes-associated protein form a dynamic complex

Amber Vogel | **Alexandra Crawford** | **Afua Nyarko**

Department of Biochemistry & Biophysics, Oregon State University, Corvallis, Oregon, USA

Correspondence
Afua Nyarko, Department of Biochemistry & Biophysics, Oregon State University, Corvallis, OR 97331, USA.
Email: nyarkoa@oregonstate.edu

Funding information
National Science Foundation, Grant/Award Number: MCB-2114544; Murdock Charitable Trust, Grant/Award Number: 2014162; National Institutes of Health, Grant/Award Number: 1S10OD018518; Oregon State University

Review Editor: Carol Beth Post

Abstract

Multivalent complexes formed between the cancer-promoting transcriptional co-activator, Yes-associated protein (YAP), and proteins containing short linear motifs of type *PPxY* modulate cell proliferation and are attractive therapeutic targets. However, challenges producing *PPxY* polypeptides containing the full binding domain has limited understanding of the assembly process. Here, we successfully produced a polypeptide containing the complete set of three *PPxY* binding sites of Angiomotin-like 1 (AMOTL1), a scaffolding protein that regulates the nucleo-cytoplasmic shuttling of YAP via *WW-PPxY* interactions. Using an array of biophysical techniques including isothermal titration calorimetry, size-exclusion chromatography coupled to multi-angle light scattering, and solution nuclear magnetic resonance spectroscopy, we show that the AMOTL1 polypeptide is partially disordered, and binds the YAP WW domains to form an ensemble of complexes of varying stabilities. The binding process is initiated by the binding of one YAP WW domain to one AMOTL1 *PPxY* motif and is completed by transient interactions of the second YAP WW domain with a second AMOTL1 *PPxY* motif to form an equilibrating mixture composed of various species having two YAP sites bound to two conjugate AMOTL1 sites. We rationalize that the transient interactions fine-tune the stability of the complex for rapid assembly and disassembly in response to changes in the local cellular environment.

KEYWORDS

Angiomotin, circular dichroism (CD), intrinsically disordered protein, isothermal titration calorimetry (ITC), multivalent, nuclear magnetic resonance spectroscopy (NMR), *PPxY*, protein–protein interaction, scaffolding protein, WW domain, Yes-associated protein

1 | INTRODUCTION

Yes-associated protein (YAP) is a transcriptional co-activator that promotes cell survival by activating cell proliferation and anti-apoptosis.[1] YAP-mediated processes are linked to various cancers in which cellular levels and nuclear localization of YAP are increased, and subsequent interactions of DNA-binding transcription factors with YAP are important first steps.[2] Given their central role in cell survival, we have undertaken foundational structure–function studies to elucidate YAP regulatory mechanisms. Results will elucidate fundamental scientific questions as well as inform the

Abbreviations: CD, circular dichroism spectroscopy; HSQC, heteronuclear single quantum coherence; ITC, isothermal titration calorimetry; NMR, nuclear magnetic resonance spectroscopy; WT, wild type.

design of novel small molecules for therapeutic intervention.

Multiple proteins are implicated in the regulation of YAP cellular concentrations and localization. Among them are the Motin family of proteins Angiomotin (AMOT), Angiomotin-like 1 (AMOTL1), and Angiomotin-like 2 (AMOTL2) which function in cell differentiation, proliferation, and migration.[3–7] The three proteins bind directly to YAP to regulate YAP-promoted cell proliferation.[5,8–12] Key to Motin interactions with YAP are 2–3 short linear motifs (SliMs) of type *L/PPxY* (hereafter referred to as *PPxY*) which recognize tandem YAP WW domains, autonomous folding units which adopt a triple-stranded beta-sheet fold and are characterized by the presence of two conserved tryptophans.[13] Here we focus on molecular interactions between YAP and AMOTL1.

AMOTL1 is a 106 kDa protein with three *PPxY* motifs (P1, P2, and P3) which precede three structured domains: a Bin/Amphiphysin/Rvs (BAR) domain, a coiled-coil (CC) domain, and a postsynaptic density protein (PDZ)-binding domain[3,14,15] (Figure 1). High structural disorder is predicted for the *PPxY* segment and challenges producing large primarily disordered fragments may explain why biophysical studies of fragments containing all three *PPxY* sites have been limiting. An attractive workaround to produce shorter polypeptides with one or two *PPxY* sites has led to conflicting reports; some studies suggest

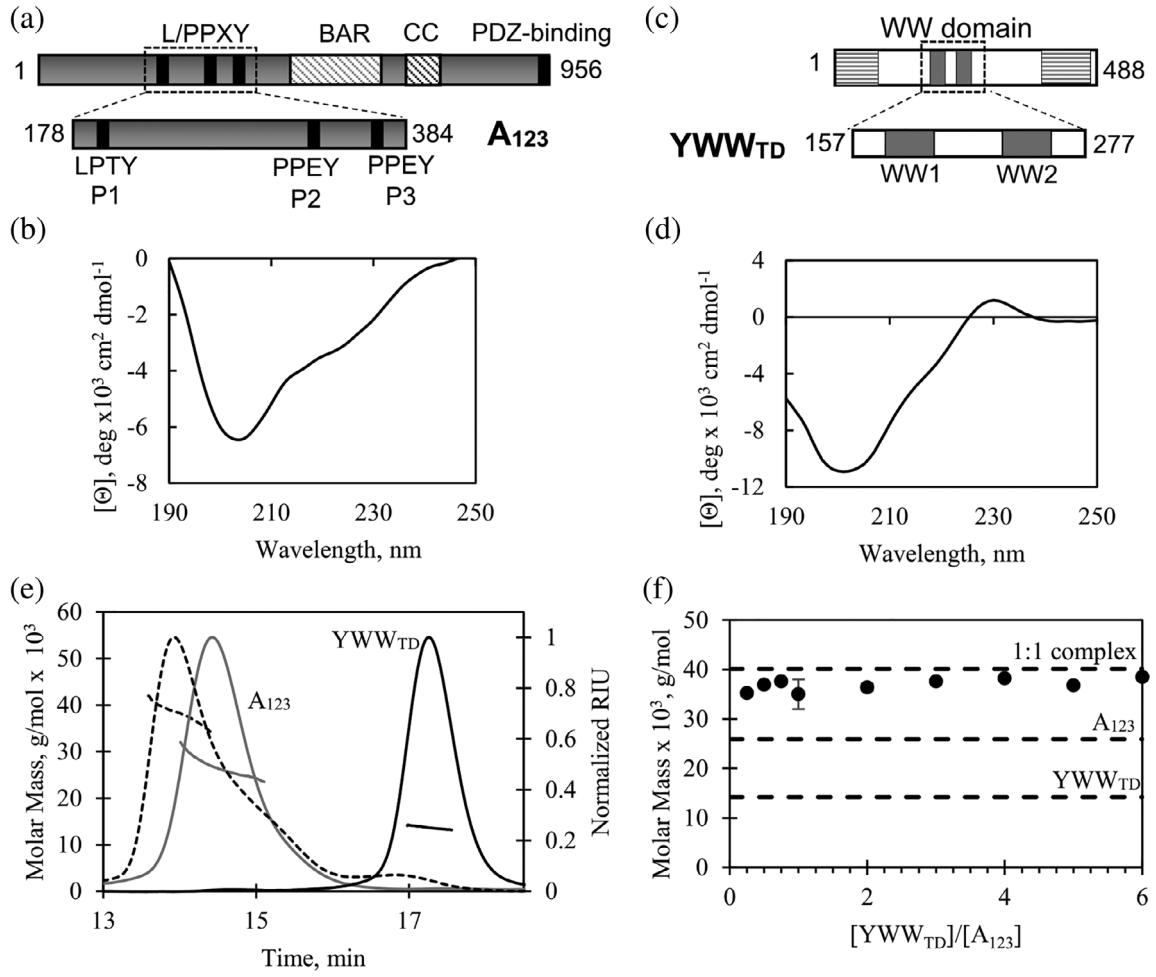

FIGURE 1 Domain architecture and solution properties of apo and bound AMOTL1 and YAP polypeptides. (a) Full-length AMOTL1 (956-residues) contains three *PPxY* motifs which precede, a Bin/Amphiphysin/Rvs (BAR), coiled-coil (CC) and a postsynaptic density protein (PDZ)-binding domains. The AMOTL1 A_{123} construct (residues 178–384) includes all three *PPxY* sites. (b) Far UV CD spectrum of A_{123} is consistent with a partially disordered polypeptide. (c) YAP, a multidomain protein, contains two WW domains, WW1 and WW2. The YAP construct, YWW_{TD} (residues 157–277) was designed to include both WW domains. (d) Far UV CD spectrum of YWW_{TD} shows the characteristic spectrum of a WW domain. (e) SEC-MALS elution profiles of A_{123} (gray line), YWW_{TD} (black line), and a 1:1 mixture of both proteins (dashed black line). (f) A plot of the SEC-MALS-detected molar mass of varying ratios of A_{123}:YWW_{TD} complexes. The average molar mass values range between 34.9–37.8 kDa. The theoretical molar masses of A_{123}, YWW_{TD}, and the 1:1 A_{123}-YWW_{TD} complex are indicated by dashed lines

that P2 is the most relevant motif[5,10,11]; and others demonstrate that both P1 and P2 sites function in complex formation.[8]

Our experiments resolve the question of which *PPxY* motifs are required for in vitro assembly of the YAP-AMOTL1 complex. A battery of formidable and mutually reinforcing molecular biophysical methodologies are employed, and the experimental results are collectively interpreted in the context of the function of the YAP-AMOTL1 complex.

2 | RESULTS

2.1 | SEC-MALS and CD experiments of apo and bound proteins

In these experiments, we use A_{123}, a multivalent 207-residue AMOTL1 polypeptide (residues 178–384) with three *PPxY* motifs—LPTY, PPEY, and PPEY (Figure 1a). The far ultra-violet (UV) circular dichroism (CD) spectrum of A_{123} (Figure 1b) shows a strong signal at 204 nm, suggestive of random coil-like structure, and a relatively weak signal at 222 nm indicative of nascent helical structure. The experimental CD spectrum was analyzed with the webserver, DichroWeb,[16,17] to provide calculated secondary structure contents of 24.7% helix, 0.6% strands, 15.9% turns, and 43.7% disordered segments.

The YAP polypeptide, YWW_{TD}, (residues 157–277, Figure 1c) contains both WW domains (WW1 and WW2). The far UV CD spectrum of YWW_{TD} (Figure 1d) shows a positive peak at 230 nm and a negative peak at 220 nm which are signature WW domain peaks attributed to the packing of the two tryptophans and the β-strands, respectively. Taken together, the CD analysis is consistent with a partially folded A_{123} polypeptide, and a largely folded YWW_{TD} polypeptide.

Size-exclusion chromatography (SEC) combined with multi-angle light scattering (MALS) can be used to determine the molar mass of a protein without the need for a column calibration curve.[18] Completely or partially disordered proteins have relatively large hydrodynamic radii, which precludes the use of SEC alone to infer molecular mass, whereas SEC-MALS is particularly attractive for computing their molar mass. The average molecular mass of A_{123} probed by SEC-MALS is 26.1 ± 1.2 kDa, a value close to the theoretical monomer molecular mass of 25.9 kDa. The SEC-MALS calculated molar mass of YWW_{TD} is 14.1 ± 1.1 kDa (expected monomer molar mass is 14.2 kDa) (Figure 1e; Table 1). An equimolar mixture of A_{123} and YWW_{TD} elutes earlier than unbound A_{123} or YWW_{TD} with an SEC-MALS-measured molecular mass of 35 kDa, slightly less than the theoretical molar mass of 40.1 kDa expected for a 1:1 complex. When resolved on SDS-PAGE, the peak for the equimolar mixture migrates as two bands with migration rates similar to unbound A_{123} and YWW_{TD} (data not shown). A_{123} and YWW_{TD} complexes formed by mixing 0.25–6-fold molar excess of YWW_{TD} with A_{123} give SEC-MALS measured molecular masses in the range 34.9–37.8 kDa (Figure 1f), values slightly less than the theoretical molar mass of 40.1 kDa for a 1:1 complex (Table 1). Taken together, the SEC-MALS data indicate that under the experimental conditions, the A_{123} and YWW_{TD} polypeptides are monomeric in solution, and the YWW_{TD}-A_{123} complex is formed between one YWW_{TD} molecule and one A_{123} molecule.

TABLE 1 Experimental and theoretical molar masses of apo and bound AMOTL1 A_{123} and YAP YWW_{TD}

		Molar mass (kDa)	
Protein	**Stoichiometry**	**Experimental**	**Theoretical**
A_{123} (AMOTL1)	–	26.1 ± 1.2[a]	25.9
YWW_{TD} (YAP)	–	14.1 ± 1.1[a]	14.2
YWW_{TD}-A_{123} complex	0.25:1	34.9	–
	0.5:1	37.3	–
	0.75:1	37.2	–
	1:1	35 ± 3[a]	40.1
	2:1	36.4 ± 0.7[a]	54.3
	3:1	36.8	68.5
	4:1	37.0	82.7
	5:1	36.8	96.9
	6:1	37.8	111.1

[a]Reported value is the average of triplicate experiments.

2.2 | Solution NMR experiments of apo and YAP-bound AMOTL1 A_{123}

NMR experiments were used to determine for A_{123} the local secondary structure propensity, backbone dynamics, and binding interface residues. The ^{1}H-^{15}N heteronuclear single quantum coherence (HSQC) spectrum of A_{123} shows poor dispersion in the NH-region, as expected for a protein with random coil-like and/or helical structure (Figure 2a). Despite significant peak overlap, we assigned 79% (145 of 183 non-proline residues) of backbone nuclei, which enabled residue-specific analyses. Resonance assignments for the 26 additional residues that are part of the expression vector are not included in the analysis.

PSIPRED,[19] a sequence-based secondary structure prediction algorithm, shows that the A_{123} polypeptide is largely disordered except for three short helical segments designated H1, H2, and H3 (Figure 2). The experimental secondary structure propensities of A_{123} were determined from the relative deviations of assigned CA and CB chemical shift values from standard random coil values (ΔCA-ΔCB). A plot of the ΔCA-ΔCB as a function of the residue number (Figure 2b), shows sequential and substantial positive values for residues 193–197, 261–263, 265–267, and 269–270, within the predicted helical segments H1 and H3. An additional stretch of residues (245–257) within the predicted H2 α-helical segment has positive deviations slightly below the computed average value of 0.4 (Figure 2b, dashed line), suggestive of a relatively weak or nascent helix. Using the backbone chemical shifts and the δ2D analysis software,[20] we determined the probability distribution of secondary structural elements as 69.1% coil, 15.8% polypropylene II helix, 8.0% regular helix, and 7.1% strands consistent with the conclusion from CD analysis that A_{123} has limited folded structure.

To identify solvent-exposed residues in the A_{123} polypeptide, a clean chemical exchange (CLEANEX)-HSQC experiment which measures fast backbone amide proton exchange with water was recorded. The plot in Figure 2c shows residues with rapidly exchanging amide protons

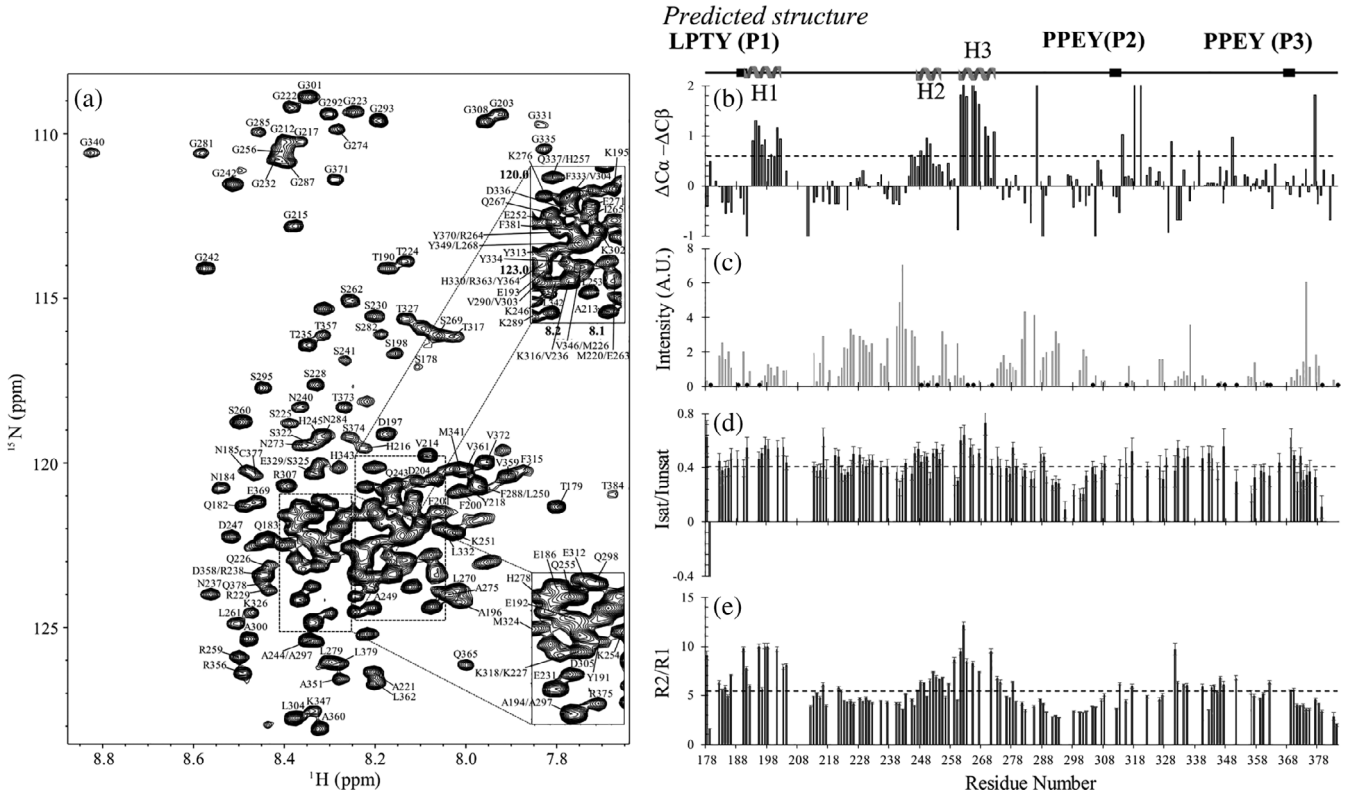

FIGURE 2 NMR backbone assignments and solution dynamics of AMOTL1 A_{123} polypeptide. (a) ^{1}H-^{15} N-HSQC of A_{123} showing assignments for 145 of 183 non-proline residues. (b) A plot of the deviation of the chemical shifts from random coil values (Δ13Cα − Δ13Cβ). (c) CLEANEX-HSQC analysis of A_{123}. The gray bars represent the rapidly exchanging amide protons, and the black dots are the relatively slow exchanging amide protons. (d) A plot of the steady-state heteronuclear NOE (Het-NOE) values. (e) The ratio of the transverse and longitudinal relaxation (R_2/R_1) as a function of the residue number. Average values are shown as dashed lines in plots b, d, and e. The predicted secondary structure of A_{123} is shown above the plots as a line diagram where disordered segments are represented by a solid line. Three predicted helices, H1 (residues 191–202) and H2 (residues 247–254), and H3 (residues 261–272) are located between the first (P1) and second (P2) PPxY sites

(gray bars) and solvent-protected residues (black circles). The latter residues are not detected in the CLEANEX-HSQC spectrum (Figure S1). As expected for a predominantly unstructured polypeptide, most residues in A_{123} are accessible to solvent, with the most rapidly exchanging amide protons (residues with the highest intensities) within the linker segments connecting the P1 and P2 sites. Consistent with a predicted helical segment, the amide protons for residues in the H2 segment are protected from solvent.

To determine backbone dynamics at multiple timescales, we measured a suite of NMR experiments, including steady-state ^{1}H-^{15}N heteronuclear NOE (HetNOE), ^{15}N longitudinal (R_1) and transverse (R_2) relaxation. HetNOE measurements are sensitive to the strength of the magnetic field and report backbone dynamics in the pico- to nanosecond (ps-ns) timescale. Generally, positive and negative HetNOE values are indicative of restricted and mobile residues respectively, but at high magnetic field strengths, mobile residues may display low positive values.[21] HetNOE values for the A_{123} polypeptide, at a magnetic field strength of 800 MHz, are mostly positive, with an average of 0.4 (Figure 2d). At this relatively low positive average value, most segments of residues are mobile. The most mobile residues, 179 and 384 (negative NOE value), are at the N and C-termini. Intriguingly, the first residue of the native protein sequence (178) has an NOE value greater than the average value of 0.4. A possible explanation for this anomaly is that the non-native poly-histidine sequence adjacent to 178 restricts the motion of this residue.

The ratio of the transverse and longitudinal relaxation (R_2/R_1) reflects motions in the nanosecond timescale and identifies segments with slower tumbling. The plot in Figure 2e shows relatively high values for residues 190–198 and 259–271 which implies relatively slower tumbling for the two segments.

A_{123} residues involved in binding YWW_{TD} were mapped by NMR titration experiments in which unlabeled YWW_{TD} and isotopically labeled A_{123} were mixed at molar ratios in the range of 0.25:1–2:1 (YWW_{TD}:A_{123}). As a reporter of the binding interactions, we monitored changes in the intensities of peaks corresponding to the tyrosine residues, Y191, Y313, and Y370, at the 3 *PPxY* sites. The plot in Figure 3a shows a decrease in the intensity of each tyrosine peak with increasing concentrations of added YWW_{TD}. Note that peaks for all three tyrosine residues are not detected in the partially bound 0.75:1 (YWW_{TD}:A_{123}) complex. Loss in peak intensity is attributed to binding-induced exchange broadening, binding-induced conformational changes and/or slower tumbling of the complex.[22] Line broadening occurs, and peaks disappear when the rate of exchange between the bound and unbound conformations is intermediate on the NMR timescale.

Complex formation also induces resonance intensity changes in other residues and leads to many missing peaks in spectra of the YAP-bound protein (Figure S2). These missing peaks imply that the residues are close to binding interfaces and/or involved in binding-induced allosteric changes.[23] At the 0.75:1 molar ratio (Figure 3b, upper panel), missing cross-peaks map to residues in the sequence vicinity of P1 (186–204), H2 (261, 265, 268 and 273), P2 (305–317), P3 (365–371), and the linker segment between P2 and P3 (322, 335, 340, 342). Additional cross-peaks corresponding to residues 245, 262–264, 269–274 and C-terminal residues 302–384 (except 328, 349, 358) are missing in the spectrum of the 1:1 YWW_{TD}-A_{123} complex (Figure 3b, middle panel). At the final molar ratio of 2:1 (YWW_{TD}: A_{123}), the only remaining spectral peaks correspond to residues primarily located in the P1-P2 linker segment (Figure 3b, lower panel).

To identify protected segments in the partially bound A_{123} polypeptide, the CLEANEX-HSQC experiment recorded for the unbound A_{123} polypeptide (Figure 2c) was compared to a CLEANEX-HSQC experiment recorded on a partially bound protein at a YWW_{TD}:A_{123} molar ratio of 0.25:1. Peaks that disappear upon addition of 0.25 molar equivalents of YWW_{TD} are mapped onto the CLEANEX-HSQC data of unbound A_{123} and are shown as cyan bars in Figure 3c. Amide protons which are most protected from the solvent map to residues in the sequence vicinity of P1, P2, P3, and the predicted H2 helical segment.

To summarize the NMR titration and CLEANEX-HSQC data, the partially bound A_{123} polypeptide formed by addition of a sub-stoichiometric concentration of YWW_{TD} to A_{123} results in disappearance of peaks in the sequence vicinity of all three *PPxY* motifs, which indicates that YWW_{TD} binds all three sites concurrently. Most of the missing peaks in the stoichiometric complex are in the sequence vicinity of the P1 site, which suggests more favorable interactions at the P1 site. Further, peaks corresponding to most residues in the predicted helix (H3), which is not a putative binding site, also disappear, possibly due to binding-induced conformational changes. Finally, spectral peaks remaining in the fully bound complex map to the linker segment between P1 and P2; an indication that residues in this linker region of A_{123} remain largely disordered in the YAP-bound protein.

2.3 | ITC experiments of WT and site-directed mutants

Reaction thermodynamics, stoichiometry, and effective binding affinity of the A_{123}-YWW_{TD} interaction were determined by ITC. Binding of the two proteins is

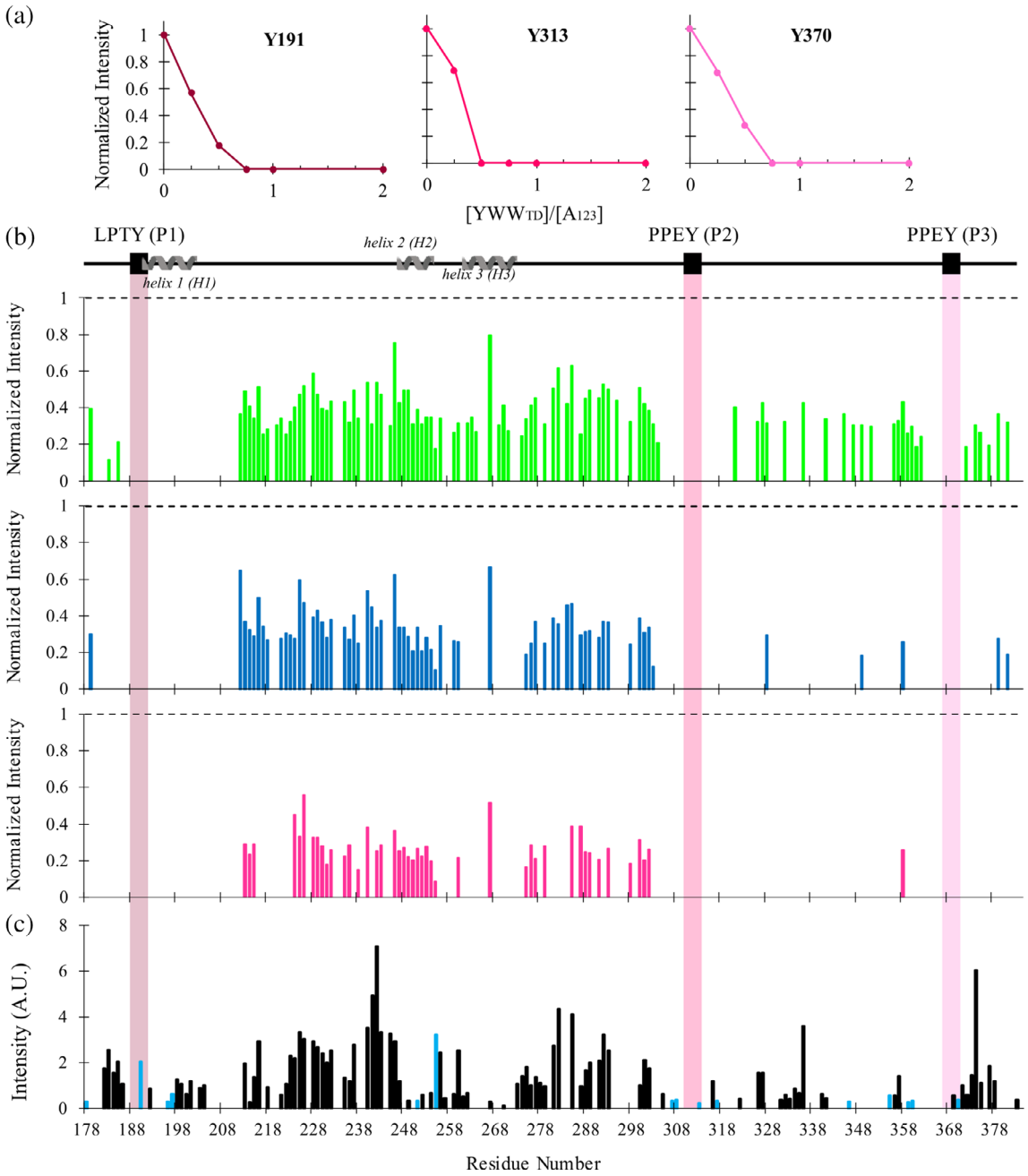

FIGURE 3 NMR mapping of the A_{123}-YWW_{TD} binding interface. (a) Changes in peak intensities of the three tyrosine residues, Y191 (P1), Y313 (P2), Y370 (P3), of each motif as a function of YWW_{TD}-A_{123} molar ratio. (b) Normalized intensities of assigned A_{123} residues plotted as a function of the residue number for apo A_{123} (black dashed lines), and upon addition of 0.75 (top panel, green), 1 (middle panel, blue), and 2 (bottom panel, magenta) molar equivalents of YWW_{TD}. The predicted secondary structure is shown above the plots. At the final molar equivalents of 2:1 (bottom panel), only residues primarily located in the P1-P2 linker segment are observed in the spectrum. (c) A bar plot of the intensities of peaks in the CLEANEX-HSQC spectrum of unbound A_{123}. Peaks that disappear upon addition of 0.25 molar equivalents of YWW_{TD} are shown in cyan and include residues at the three PPxY sites (shaded in pink)

enthalpically driven, occurs with a binding stoichiometry (N) close to 1:1 and has an effective dissociation constant (K_d) of 0.26 ± 0.01 μM (Figure 4a; Table 2). Because there are two putative binding sites on the YWW_{TD} polypeptide (2 WW domains) and three putative binding sites on the A_{123} polypeptide (3 *PPxY* motifs), binding of a single WW-*PPxY* site or of both WW sites to two *PPxY* sites will result in a binding stoichiometry of 1:1.

To determine whether a single YAP WW domain is sufficient for binding, we introduced mutations that inactivate either the first ($P202A_{TD}$) or second ($P261A_{TD}$) YAP WW domain. Binding of A_{123} to the $P202A_{TD}$

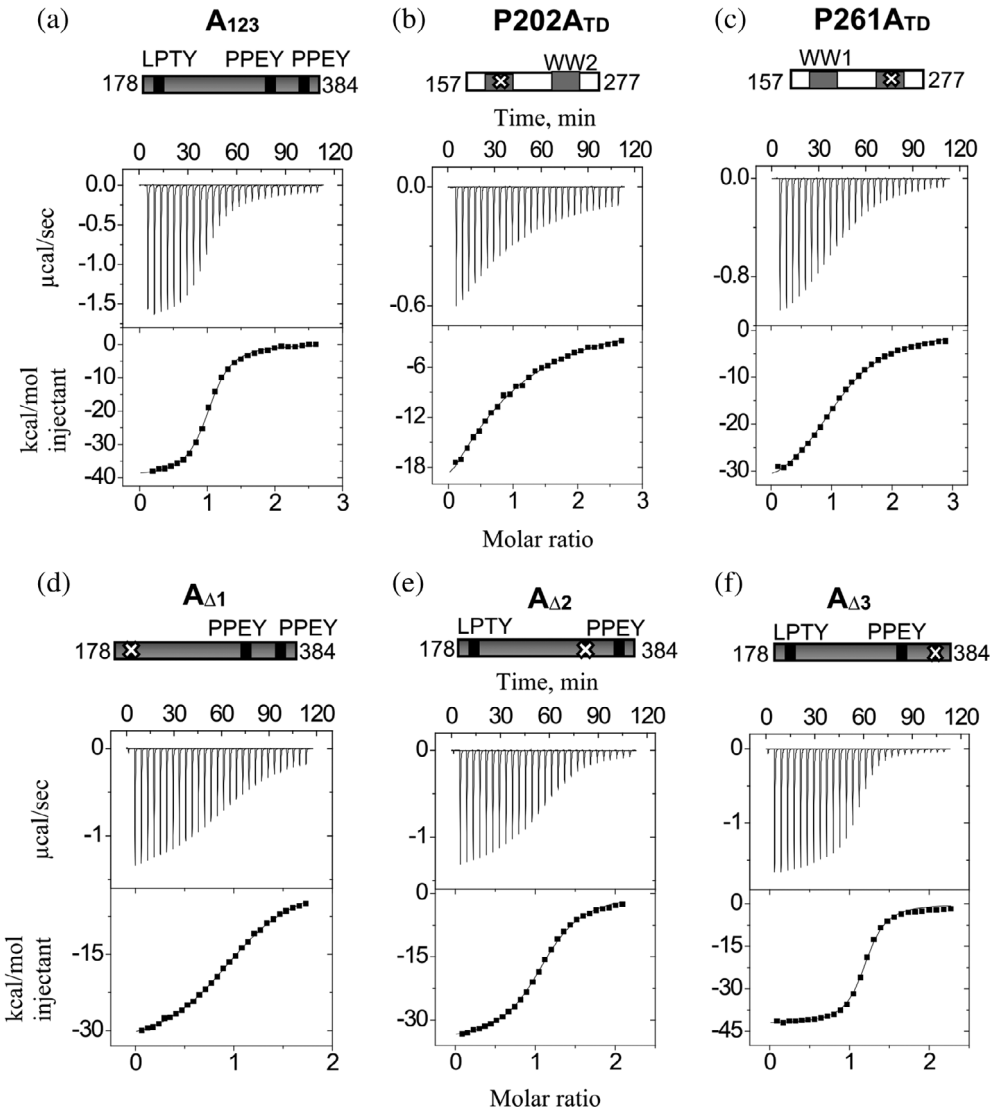

FIGURE 4 ITC binding isotherms of the A_{123}-YWW_{TD} interaction. Representative binding isotherms for interactions of A_{123} with (a) YWW_{TD} (b) $P202A_{TD}$ and (c) $P261A_{TD}$ or YWW_{TD} with A_{123} mutants (d) $A_{\Delta1}$, (e) $A_{\Delta2}$ (f) $A_{\Delta3}$ in which sites P1, P2 and P3, respectively are inactivated. Active domains or motifs are labeled in the schematic of the constructs above each binding isotherm. ITC data were collected at 25°C in pH 7.5 buffer composed of 50 mM sodium phosphate, 50 mM NaCl, 5 mM β-mercaptoethanol, and 0.5 mM NaN_3

TABLE 2 Thermodynamics parameters for the YAP-AMOTL1 interactions

Titrant	Cell	*N*	K_d (μM)	ΔH (kcal/Mol)	TΔS (kcal/Mol)	ΔG (kcal/Mol)
YWW_{TD}	A_{123}	1.1	0.26 ± 0.01	−39.6 ± 0.9	−30.3 ± 0.9	−8.98 ± 0.03
	$A_{\Delta1}$[a]	1.0	1.8	−33.8	−26.0	−7.8
	$A_{\Delta2}$	1.1	0.6 ± 0.1	−35.5 ± 0.3	−27.1 ± 0.3	−8.47 ± 0.01
	$A_{\Delta3}$[a]	1.2	0.11	−41.1	−31.8	−9.5
$P202A_{TD}$	A_{123}	1.0	7.6 ± 0.2	−37 ± 4	−30 ± 4	−6.98 ± 0.01
$P261A_{TD}$	A_{123}	1.2	0.70 ± 0.02	−30 ± 2	−22 ± 2	−8.40 ± 0.02

[a]Reported value is the average of duplicate experiments. All other values are the average of triplicate experiments.

mutant occurs with a K_d of 7.6 μM (Figure 4b), a value ~10-fold higher than 0.7 μM computed for the A_{123}-$P261A_{TD}$ interaction (Figure 4c). The binding stoichiometry of 1:1 or 1:1.2 implies that in each case the active WW domain binds at least one A_{123} *PPxY*. However, the weaker but significantly different binding affinities of the mutants relative to the WT YWW_{TD} polypeptide suggest that both YAP WW domains contribute to the stability of the WT YWW_{TD}:A_{123} complex.

To determine if inactivating specific *PPxY* sites destabilizes the A_{123}-YWW_{TD} complex, we used A_{123} "knockout" variants, $A_{\Delta1}$, $A_{\Delta2}$, and $A_{\Delta3}$, each with one inactivated motif (indicated by subscript). Figures 4d–f show that the reactions are enthalpically driven and have

a binding stoichiometry in the range of 1:1 to 1:1.2 for each "knockout" site (Table 2). The effective K_d varies from 1.8 μM in $A_{\Delta 1}$ (Figure 4d) to 0.6 μM in $A_{\Delta 2}$ (Figure 4e) and 0.1 μM in $A_{\Delta 3}$ (Figure 4f; Table 2). In summary, the binding of YWW_{TD} to A_{123} is more stable (lower K_d) when both the YAP WW1 domain and AMOTL1 P1 sites are active. Inactivating the P2 site leads to a modest decrease (higher K_d) in the stability of the complex, while inactivating the P3 site has the opposite effect, that is, a modest increase (lower K_d) in the stability of the complex. Finally, the non-integer binding stoichiometries are indicative of inhomogeneity in the complexes formed, possibly due to variations in the number of occupied binding sites.

3 | DISCUSSION

Direct binding of the AMOTL1 scaffold protein to YAP regulates cell proliferation. While it is known that assembly of the complex occurs via multivalent WW-*PPxY* interactions, and studies with shorter polypeptides containing one or two *PPxY* sites have provided some insight into the binding interactions, it remains unknown how polypeptides containing the full binding domain interact, specifically which pairs of the three *PPxY* sites bind the two YAP WW domains. We have clarified the uncertainty as to which AMOTL1 *PPxY* motifs are required for the assembly of its complex with YAP. Our first advancement was to produce a construct of AMOTL1 (A_{123}), which contains the entire multivalent *PPxY* segment rather than only one or two *PPxY* sites, and to use site-directed mutagenesis of A_{123} to inactivate specific *PPxY* sites. Then we characterized interactions of the tandem WW domains of YAP (YWW_{TD}) with A_{123} and its *PPxY* variants. Our conclusions are drawn from collective analyses of data measured by an extensive array of methodologies applied both to apo proteins and to the complex formed by A_{123} and YWW_{TD}.

We conclude that the apo AMOTL1 *PPxY* domain, A_{123}, has a limited folded structure, localized in two short helical segments, residues 193–197 and 245–257 as shown by CD and NMR. This first experimental demonstration that the full AMOTL1 *PPxY* segment is partially disordered is consistent with the structures of other multivalent *PPxY* proteins.[24–26] Second, the AMOTL1-YAP *PPxY-WW* complex is formed by one molecule of AMOTL1 bound to one molecule of YAP, as shown by the hydrodynamic method of SEC-MALS and ITC. Third, binding of the YAP tandem WW domains to A_{123} perturbs residues at all three *PPxY* sites as shown by solution NMR spectroscopy. More residues are perturbed in the sequence vicinity of the P1 site, a clear indication of more intermolecular interactions at P1 relative to P2 or P3, and evidence that P1 is critical for the assembly of the AMOTL1-YAP complex. The P1 site in the AMOTL1 paralog, AMOT, is also indispensable for binding specific WW domain targets[8] and plays a critical role in the function of the protein.[27] Likewise, the P1 site in AMOTL1 may provide some functional advantages to the protein. Fourth, inactivating the P3 site results in a ~2-fold binding enhancement which implies that P3 contributes negative entropy to the overall interaction. We speculate that the negative entropy may be eliminated when the P3 site is occupied by another WW domain protein such as the kidney and brain expressed protein KIBRA, which is reported to preferentially bind the P3 site in AMOT.[7] Inactivating the YAP WW1 domain also de-stabilized the complex to a much greater degree than the WW2 domain, findings in agreement with the different binding preferences of the YAP WW domains.[28]

Considered together, the novel information from these complementary methodologies indicates that the AMOTL1-YAP *PPxY-WW* complex is structurally dynamic, and the YAP WW tandems interact with all three *PPxY* sites in AMOTL1 as illustrated by the model in Figure 5. The dynamic structure is composed of different complexes of varying stabilities as previously noted for other *WW-PPxY* complexes.[24,26] Complexes in which the YAP WW domains bind AMOTL1 sites P1-P2 or P1-P3 are the most stable; and the least stable complex is formed by relatively weak or transient binding of the YAP WW domains to AMOTL1 sites P2-P3. Simultaneous binding of both YAP WW domains to varying pairs of AMOTL1 *PPxY* sites leads to the formation of an equilibrating mixture of interconverting species transiently formed by two YAP sites bound to two conjugate AMOTL1 sites.

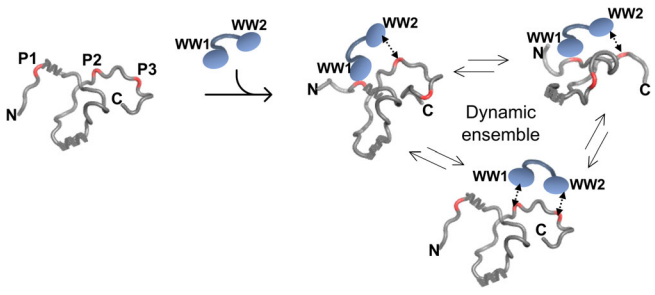

FIGURE 5 Model of the species formed in the AMOTL1-YAP complex. The YAP tandem WW domains and the predominantly unstructured AMOTL1 PPxY domain-containing three PPxY sites, designated P1, P2, and P3, form a dynamic ensemble of interconverting complexes. Complexes in which AMOTL1 sites P1-P2 or P1-P3 are bound are relatively more stable than the complex in which sites P2-P3 are bound

3.1 | Functional implications of a dynamic YAP-AMOTL1 complex

A hallmark of regulatory complexes in signaling pathways is their rapid and spontaneous response to cellular signals. The modest micromolar binding affinity of the dynamic complex can facilitate rapid assembly and disassembly of the complex in response to changes in the local environment. Further, recent findings that link YAP,[29] multivalency, intrinsic disorder, and low complexity regions, to phase separation and the formation of membraneless organelles in human cells[30–33] could organize the ensemble in space. Phase separation may be triggered by changes in the local environment such as a change in the local concentration of YAP. The presence of another WW domain-containing protein could also shift the dynamic equilibria in favor of specific complexes. For instance, AMOTL1 forms a ternary via *WW-PPxY* interactions with both YAP and the kidney and brain expressed protein KIBRA[34]; and simultaneous binding to both WW domain partners may shift the dynamic equilibria in favor of specific complexes in the ensemble. We propose that forming dynamic complexes underlie AMOTL1 function.

4 | MATERIALS AND METHODS

4.1 | Cloning of constructs

The genes encoding AMOTL1 (Uniprot ID Q8IY63, residues 178–384, designated A_{123}) and YAP, (Uniprot ID P46937-2, residues 157–277, designated YWW_{TD}) were inserted into a modified pET24 vector (Millipore-Sigma, MA, USA) with an N-terminal His_6 tag and a tobacco-etch virus (TEV) protease cleavage site. A_{123} mutants with a single Tyr to Ala substitution of the first (Y191A, designated $A_{\Delta1}$), second (Y313A, designated $A_{\Delta2}$), or third (Y370A, designated $A_{\Delta3}$) *L/PPxY* motif; YWW_{TD} mutants with Pro to Ala substitutions in the first ($P202A_{TD}$) or second ($P261A_{TD}$) WW domains were generated using the Q5® site-directed mutagenesis kit (New England Biolabs, MA). Tyr to Ala substitutions in *L/PPxY* motifs or Pro to Ala substitutions in WW domains inactivate the mutant *L/PPxY* motif or WW domain.[25,35] The YAP cDNA was a gift from Kunliang Guan (Addgene plasmid # 24637).

4.2 | Recombinant protein production

Escherichia coli BL21 (DE3) cells with the gene of interest were cultured at 37°C in terrific broth (A_{123} proteins) or lysogeny broth (YWW_{TD} proteins). For isotopically labeled proteins, cells were cultured in MJ9 supplemented with $^{15}NH_4Cl$ and ^{12}C or ^{13}C glucose. Proteins were overexpressed at 20°C for 5 (A_{123} variants) or 16 (YWW_{TD} proteins) hours after induction with 0.1 mM IPTG. His_6-tagged recombinant proteins were purified as previously reported.[25] The A_{123} polypeptides were prone to proteolytic degradation, therefore, to minimize degradation the purification tag which is part of the expression vector was not removed from the N-terminal end of the polypeptide. This introduced 26 non-native residues to the N-terminal end of the A_{123} polypeptides. A_{123} proteins expressed in MJ9 accumulated in inclusion bodies and were purified following protocols described elsewhere.[36] Protein concentrations were determined from the absorbance at 280 nm and extinction coefficient values computed from the protein sequence (http://web.expasy.org/protparam/).

4.3 | Circular dichroism

Far UV circular dichroism (CD) measurements were recorded at 25°C on a JASCO 720 spectrophotometer using a path length of 1 mm, and a bandwidth of 1.0 nm. Prior to data collection, the protein was dialyzed against 10 mM sodium phosphate, pH 7.5 with or without 100 mM NaF. The final concentration of the protein for CD analysis was 3 or 5.4 μM and reported CD data are the average of experimental repeats.

4.4 | Size-exclusion chromatography-multi-angle light scattering (SEC-MALS)

The average molar masses and association states of the proteins were determined from SEC (AKTA FPLC; GE Healthcare) connected to multi-angle light scattering (DAWN; Wyatt Technology) and refractive index (Optilab; Wyatt Technology) detectors. 100 μL of proteins in the concentration range of 25–150 μM were injected at a flow rate of 0.7 or 1.0 mL/min onto a $Superdex^{200}$ 10/300 (Cytiva life sciences) chromatographic column pre-equilibrated with a pH 7.5 buffer composed of 50 mM sodium phosphate, 0.4 M NaCl, 1 mM NaN_3, 5 mM β-mercaptoethanol. Average molar masses were computed with the ASTRA software package, version 8 (Wyatt Technologies).

4.5 | NMR data collection and analysis

NMR experiments were performed at 10°C on a Bruker Avance III, 800 MHz spectrometer (Bruker BioSpin) equipped with a triple resonance cryogenic probe. Data

were collected on isotopically labeled A_{123} at concentrations of 75 or 200 μM and in a pH 6.8 buffer composed of 50 mM sodium phosphate, 100 mM NaCl, 50 mM arginine, 50 mM glutamate, 1 mM NaN_3, and 2 mM tris (2-carboxyethyl) phosphine. All samples contained 10% D_2O as the lock nucleus and 0.5% DSS for internal referencing.

Backbone resonances were assigned from BEST-TROSY ^1H-^{15}N HSQC experiments[37] and triple resonance (3D) experiments HNCACB, HN(CO)CACB, HNCO, HN(CA)CO, and ^1H-^{15}N HSQC-TOCSY. The TROSY-based pulse sequences were used to reduce line broadening due to rapid signal decay. All 3D experiments used non-uniform sampling (NUS) to reduce data collection times. The NUS data were reconstructed using the iterative shrinkage thresholding approach in NMRPipe.[38] NMR spectra were processed in NMRPipe[38] and visualized with Sparky[39] or NMRView.[40]

Per-residue secondary structure propensities were calculated from the deviations of experimental CA and CB chemical shifts from the random coil values of Poulsen et al (https://spin.niddk.nih.gov/bax/nmrserver/Poulsen_rc_CS/).[41–43] Substantial positive deviations greater than a pre-determined mean value, for four or more sequential residues indicate helical propensity while negative deviations for three or more sequential residues suggest an extended structure.

Heteronuclear NOE (HetNOE), longitudinal (R_1), and transverse (R_2) spin relaxation rates were measured using TROSY-based interleaved pulse sequences.[44] HetNOE experiments were collected with and without proton saturation using a relaxation delay of 8 s. NOE errors were calculated as previously reported.[25] R_1 spin relaxation rates were measured with relaxation delays of 0.02, 0.06 (×3), 0.1, 0.2, 0.4, 0.6, 0.8, and 1.2 s. R_2 spin relaxation rates were obtained with delays of 17, 34 (×3), 51, 68, 85, 140, 170, and 240 ms with a recycle delay of 1.5 s. R_1 and R_2 data were fit to a single exponential decay function, $I(t) = I_0 e^{-Rt}$, where t is the variable relaxation delay and R is the relaxation rate. Rates were computed using the rate analysis tool in NMRView.[40] Experimental errors were estimated from standard deviations of triplicate (×3) experiments. Results are reported only for unambiguously assigned resonances with reliably quantified peak intensities.

CLEANEX NMR experiments were collected with a mixing time of 100 ms using a recycle delay of 1.5 s. The A_{123}-YWW_{TD} complex was formed by adding 0.25 molar equivalents of YWW_{TD} to A_{123}.

For NMR titration experiments, unlabeled YWW_{TD} was added to ^{15}N-labeled A_{123} to final molar ratios (unlabeled: ^{15}N-labeled:) of 0.25:1, 0.5:1, 0.75:1, 1:1, and 2:1. To correct for minor variations in sample concentrations at each molar ratio, peak intensities (measured as peak height) were normalized as the ratio of the intensity of the peak in the bound spectrum to the intensity of the peak in the unbound spectrum.

4.6 | Isothermal titration calorimetry (ITC)

A VP-ITC instrument (Malvern Instruments Inc., MA) set to 25°C, was used to record ITC data. Prior to the titrations, all samples were extensively dialyzed against a pH 7.5 buffer composed of 50 mM sodium phosphate, 50 mM NaCl, 0.5 mM NaN_3, and 5 mM β-mercaptoethanol. Twenty seven or 28 injections of 96–148 μM WW proteins were titrated into 6–16 μM A_{123} or its variants. Data were collected in duplicates, triplicates, or quadruplicates, using proteins from two different preparations. Reported data are the average of experimental repeats. Isotherms were analyzed by single-site fits of the thermograms using the *Origin 7.1* software. The free energy of binding (ΔG) was calculated from the equation $\Delta G = -RT\ln(K_a)$, where R is the universal gas constant, T is temperature in Kelvin, and K_a is the association constant.

4.7 | delta2D method

The residue-level disorder probability of A_{123} was calculated with CA, CB, CO, N, and HN chemical shifts using the delta2D web server.[20]

4.8 | DichroWeb method

The percent helicity of A_{123} was calculated using DichroWeb[17] with data collected at 25°C on a 5.4 μM sample in buffer composed of 10 mM sodium phosphate and 100 mM NaF at pH 7.5. Reported helicity was obtained the Contin-LL method and the reference set SP175.[45]

ACKNOWLEDGMENTS

The authors wish to thank Profs. Clare Woodward and Elisar Barbar for valuable discussions, and Prof. Joachim Kremerskothen (University Hospital, Münster, Germany) for the AMOTL1 cDNA. This work is supported in part by the National Science Foundation (MCB-2114544 to A.N.) and the Christopher and Catherine Matthews Graduate Fellowship (to A.V.). NMR experiments were collected at the Oregon State University NMR Facility funded in part by the National Institutes of Health, HEI

Grant 1S10OD018518, and by the M.J. Murdock Charitable Trust grant # 2014162.

CONFLICT OF INTEREST

The authors declare that they have no conflicts of interest with the contents of this article.

AUTHOR CONTRIBUTIONS

Amber Vogel: Conceptualization (equal); formal analysis (equal); investigation (lead); methodology (equal); validation (equal); visualization (equal); writing – original draft (equal); writing – review and editing (equal). **Alexandra Crawford:** Investigation (supporting). **Afua Nyarko:** Conceptualization (lead); formal analysis (equal); funding acquisition (lead); methodology (equal); project administration (lead); resources (lead); supervision (lead); validation (equal); visualization (equal); writing – original draft (equal); writing – review and editing (lead).

DATA DEPOSITION

NMR chemical shifts for AMOTL1 (residues 178–384) have been deposited in the Biological Magnetic Resonance Data Bank (BMRB) under accession code 51029.

ORCID

Afua Nyarko https://orcid.org/0000-0002-0998-3707

REFERENCES

1. Dong J, Feldmann G, Huang J, et al. Elucidation of a universal size-control mechanism in drosophila and mammals. Cell. 2007;130:1120–1133.
2. Abylkassov R, Xie Y. Role of yes-associated protein in cancer: An update. Oncol Lett. 2016;12:2277–2282.
3. Huang T, Zhou Y, Zhang J, et al. The physiological role of Motin family and its dysregulation in tumorigenesis. J Transl Med. 2018;16:98.
4. Mana-Capelli S, McCollum D. Angiomotins stimulate LATS kinase autophosphorylation and act as scaffolds that promote hippo signaling. J Biol Chem. 2018;293:18230–18241.
5. Chan SW, Lim CJ, Chong YF, Pobbati AV, Huang C, Hong W. Hippo pathway-independent restriction of TAZ and YAP by angiomotin. J Biol Chem. 2011;286:7018–7026.
6. Ernkvist M, Birot O, Sinha I, et al. Differential roles of p80- and p130-angiomotin in the switch between migration and stabilization of endothelial cells. Biochim Biophys Acta. 2008; 1783:429–437.
7. Hirate Y, Hirahara S, Inoue K, et al. Polarity-dependent distribution of angiomotin localizes hippo signaling in preimplantation embryos. Curr Biol. 2013;23:1181–1194.
8. Yi C, Shen Z, Stemmer-Rachamimov A, et al. The p130 isoform of angiomotin is required for yap-mediated hepatic epithelial cell proliferation and tumorigenesis. Sci Signal. 2013;6:ra77.
9. Wang W, Huang J, Chen J. Angiomotin-like proteins associate with and negatively regulate YAP1. J Biol Chem. 2011;286: 4364–4370.
10. Zhao B, Li L, Lu Q, et al. Angiomotin is a novel hippo pathway component that inhibits YAP oncoprotein. Genes Dev. 2011;25: 51–63.
11. Oka T, Schmitt AP, Sudol M. Opposing roles of angiomotin-like-1 and zona occludens-2 on pro-apoptotic function of YAP. Oncogene. 2012;31:128–134.
12. Ragni CV, Diguet N, Le Garrec JF, et al. Amotl1 mediates sequestration of the hippo effector Yap1 downstream of Fat4 to restrict heart growth. Nat Commun. 2017;8:14582.
13. Bork P, Sudol M. The WW domain: A signalling site in dystrophin? Trends Biochem Sci. 1994;19:531–533.
14. Moleirinho S, Guerrant W, Kissil JL. The Angiomotins--from discovery to function. FEBS Lett. 2014;588:2693–2703.
15. Mana-Capelli S, Paramasivam M, Dutta S, McCollum D. Angiomotins link F-Actin architecture to hippo pathway signaling. Mol Biol Cell. 2014;25:1676–1685.
16. Whitmore L, Wallace BA. DICHROWEB, an online server for protein secondary structure analyses from circular dichroism spectroscopic data. Nucleic Acids Res. 2004;32:W668–W673.
17. Miles AJ, Ramalli SG, Wallace BA. DichroWeb, a website for calculating protein secondary structure from circular dichroism spectroscopic data. Protein Sci. 2022;31:37–46.
18. Arakawa T, Wen J. Size-Exclusion Chromatography with On-Line Light Scattering. Current Protocols in Protein Science 2001;25(1):20–26.
19. McGuffin LJ, Bryson K, Jones DT. The PSIPRED protein structure prediction server. Bioinformatics. 2000;16:404–405.
20. Camilloni C, De Simone A, Vranken WF, Vendruscolo M. Determination of secondary structure populations in disordered states of proteins using nuclear magnetic resonance chemical shifts. Biochemistry. 2012;51:2224–2231.
21. Bolik-Coulon N, Bouvignies G, Carlier L, Ferrage F. Chapter 3 - Experimental characterization of the dynamics of IDPs and IDRs by NMR. In: Salvi N, editor. Intrinsically disordered proteins. Cambridge, MA: Academic Press, 2019; p. 65–92.
22. Cavanagh J, Fairbrother WJ, Palmer AG III, Skelton NJ. Protein NMR spectroscopy: Principles and practice, 2, Cambridge, MA: Academic Press, 2006.
23. Williamson MP. Using chemical shift perturbation to characterise ligand binding. Prog Nuclear Magn Reson Spectrosc. 2013;73:1–16.
24. Baker K, Kwok E, Reardon P, et al. Yorkie-warts complexes are an ensemble of interconverting conformers formed by multivalent interactions. J Mol Biol. 2021;433:166776–166788.
25. Kwok E, Rodriguez DJ, Kremerskothen J, Nyarko A. Intrinsic disorder and amino acid specificity modulate binding of the WW2 domain in kidney and brain protein (KIBRA) to synaptopodin. J Biol Chem. 2019;294:17383–17394.
26. Nyarko A. Differential binding affinities and allosteric conformational changes underlie interactions of Yorkie and a multivalent PPxY partner. Biochemistry. 2018;57:547–556.
27. Rheinemann L, Thompson T, Mercenne G, et al. Interactions between AMOT PPxY motifs and NEDD4L WW domains function in HIV-1 release. J Biol Chem. 2021;297:100975.
28. Iglesias-Bexiga M, Castillo F, Cobos ES, Oka T, Sudol M, Luque I. WW domains of the yes-kinase-associated-protein (YAP) transcriptional regulator behave as independent units with different binding preferences for PPxY motif-containing ligands. PLoS One. 2015;10:e0113828.

29. Cai D, Feliciano D, Dong P, et al. Phase separation of YAP reorganizes genome topology for long-term YAP target gene expression. Nat Cell Biol. 2019;21:1578–1589.
30. Banani SF, Lee HO, Hyman AA, Rosen MK. Biomolecular condensates: Organizers of cellular biochemistry. Nat Rev Mol Cell Biol. 2017;18:285–298.
31. Mitrea DM, Kriwacki RW. Phase separation in biology; functional organization of a higher order. Cell Commun Signal. 2016;14:1.
32. Martin EW, Mittag T. Relationship of sequence and phase separation in protein low-complexity regions. Biochemistry. 2018; 57:2478–2487.
33. Harmon TS, Holehouse AS, Rosen MK, Pappu RV. Intrinsically disordered linkers determine the interplay between phase separation and gelation in multivalent proteins. Elife. 2017;6:e30294.
34. Hermann A, Wennmann DO, Gromnitza S, et al. WW and C2 domain-containing proteins regulate hepatic cell differentiation and tumorigenesis through the hippo signaling pathway. Hepatology. 2018;67:1546–1559.
35. Chen HI, Einbond A, Kwak SJ, et al. Characterization of the WW domain of human yes-associated protein and its polyproline-containing ligands. J Biol Chem. 1997;272:17070–17077.
36. Nyarko A, Hare M, Hays T, Barbar E. The intermediate chain of cytoplasmic dynein is partially disordered and gains structure upon binding light chain LC8. Biochemistry. 2004;43: 15595–15603.
37. Favier A, Brutscher B. Recovering lost magnetization: Polarization enhancement in biomolecular NMR. J Biomol NMR. 2011; 49:9–15.
38. Delaglio F, Grzesiek S, Vuister GW, Zhu G, Pfeifer J, Bax A. NMRPipe: A multidimensional spectral processing system based on UNIX pipes. J Biomol NMR. 1995;6:277–293.
39. Lee W, Tonelli M, Markley JL. NMRFAM-SPARKY: Enhanced software for biomolecular NMR spectroscopy. Bioinformatics. 2015;31:1325–1327.
40. Johnson BA. Using NMRView to visualize and analyze the NMR spectra of macromolecules. Methods Mol Biol. 2004;278: 313–352.
41. Kjaergaard M, Brander S, Poulsen FM. Random coil chemical shift for intrinsically disordered proteins: Effects of temperature and pH. J Biomol NMR. 2011;49:139–149.
42. Kjaergaard M, Poulsen FM. Sequence correction of random coil chemical shifts: Correlation between neighbor correction factors and changes in the Ramachandran distribution. J Biomol NMR. 2011;50:157–165.
43. Schwarzinger S, Kroon GJ, Foss TR, Chung J, Wright PE, Dyson HJ. Sequence-dependent correction of random coil NMR chemical shifts. J Am Chem Soc. 2001;123:2970–2978.
44. Zhu G, Xia Y, Nicholson LK, Sze KH. Protein dynamics measurements by TROSY-based NMR experiments. J Magn Reson. 2000;143:423–426.
45. Lees JG, Miles AJ, Wien F, Wallace BA. A reference database for circular dichroism spectroscopy covering fold and secondary structure space. Bioinformatics. 2006;22:1955–1962.

SUPPORTING INFORMATION

Additional supporting information may be found in the online version of the article at the publisher's website.

How to cite this article: Vogel A, Crawford A, Nyarko A. Multivalent Angiomotin-like 1 and Yes-associated protein form a dynamic complex. Protein Science. 2022;31(5):e4295. https://doi.org/10.1002/pro.4295